Co-optimization Scheduling of Interdependent Power and Gas Systems with Electricity and Gas Uncertainties

Chuan Hea, Lei Wub, Tianqi Liua, Wei Weic, Cheng Wangd

°College of Electrical Engineering and Information Technology, Sichuan University, Chengdu, 610065, China

bDepartment of Electrical and Computer Engineering, Clarkson University, Potsdam, 13699, USA

cState Key Laboratory of Power Systems, Department of Electrical Engineering, Tsinghua University, 100084 Beijing, China
dState Key Laboratory of Alternate Electrical Power System with Renewable Energy Sources, North China Electric Power University, Beijing 102206, China

Abstract

The rapid growth of natural gas fuel consumption by gas-fired generators and the new emerging power-to-gas technology have intensified interdependency of electric power and natural gas systems. Consequently, such interdependency, together with heterogeneous uncertainties of the power system (e.g., power loads and renewable energy) and the gas system (e.g., gas loads), has brought new challenges to energy system operators for the secure and economic operation of interdependent power and gas systems. Specifically, uncertainties from one infrastructure could easily spread to the other, which consequently increase vulnerability and eventually lead to cascading outages of both systems. This paper proposes a two-stage adjustable robust model to study day-ahead coordinated optimal scheduling of the interdependent power and gas systems. Dual-fuel generating units are also considered for shaving gas fuel consumptions and ensuring the security of both systems during peak gas demand hours. Moreover, Weymouth gas flow constraints are linearized via Taylor series expansion, which facilitates the implementation of column-and-constraint generation algorithm to effectively solve the proposed two-stage adjustable robust model with nonlinear gas flow constraints in the second stage. Numerical case studies illustrate that dual-fuel units can enhance the secure and economical operation of interdependent power and gas systems, especially when natural gas demands present upward uncertainties. It is also demonstrated that power-to-gas facilities can facilitate a deeper penetration of volatile renewable energy by effectively converting excessive renewable generation into natural gas.

Keywords: Inderdependency; day-ahead scheduling; power-to-gas; dual-fuel; secure and economical operation; robust optimization

Nomenclature		D. Variables:	
A. Acronyms:		\mathbf{r}^{b} \mathbf{r}^{b}	
CCG	Column-and-constraint generation.	E^b_{pt} , E^b_{st}	Base-case storage volume of inactive pipeline
DC	Direct current.		p/ storage facility s at time t .
HHV	Higher heating value.	f_{pt}^+, f_{pt}^-	Binary variables indicating gas flow direction
IPGS	Interdependent power and gas systems.	J pt , J pt	
LP	Linear programing.	_	of inactive pipeline p at time t .
MILP	Mixed-integer linear programing.	$F_{it}^{b,\text{gas}}, F_{it}^{b,\text{fuel}}$	Base-case gas/ traditional fuel consumption of
PtG	Power-to-gas.	u i	unit i at time t .
UC	Unit commitment.	h	
B. Indices:		G_{jt}^b	Base-case gas production of gas well j at time t .
a, j, g, s	Indices of PtG facilities, natural gas wells, gas loads, and gas storage facilities.	$G_{pt}^{b,\text{in}}$, $G_{pt}^{b,\text{out}}$	Base-case inflow/outflow of pipeline p at time
e, m	Indices of power buses and natural gas nodes.		t.
l, p t, i, h, d, w	Indices of transmission lines and gas pipelines. Indices of hours, generating units, curve	G_{it}^b	Base-case gas consumption of unit i at time t .
	segments, power loads, and wind farms.	G_{at}^b	Base-case gas production of PtG facility a at
C. Sets and Functions:			time t.
GU,DF,TU	Set of gas-fired/dual-fuel/traditional units.	$G_{\rm st}^{b, \rm in}$, $G_{\rm st}^{b, \rm out}$	
N(e), $G(m)$	Set of components connected to power bus e	G_{st} , G_{st}	Base-case gas inflow/outflow of gas storage
	/gas node <i>m</i> .		facility s at time t .
s(l), r(l)	Set of sending/receiving buses of line <i>l</i> .	\tilde{C}_{j} , \tilde{z}	Base-case average gas flow/pressure of
Ω_P,Ω_C	Set of inactive pipelines/active pipelines with	. '	pipeline p at time t .
1	compressors.		pipeline p at time t .
Ω_D,Ω_W,Ω	G Uncertainty set of power loads/ wind	I_{it} , I_{at}	Commitment status of unit i /PtG facility a at
D · W ·	generations/ gas loads.		time t.
$\boldsymbol{\mathit{L}}^{\mathrm{pg}}\left(ullet$	Compact form of IPGS operation constraints.	I_{it}^{gas}	Binary indicator which is 1 if unit <i>i</i> burns gas at
- (compact form of it do operation constraints.	••	time t , and otherwise 0.
			time t, and otherwise o.

I_{it}^{fuel}	Binary indicator which is 1 if unit i burns traditional fuel at time t , and otherwise 0.
P_{it}^b , P_{at}^b	Base-case dispatch of unit i / PtG facility a at time t .
$P_{iht}^{b,gas}$, $P_{iht}^{b,fuel}$	Base-case dispatch of unit <i>i</i> at segment <i>h</i> at time <i>t</i> when burning gas/traditional fuel.
P_{lt}^b , θ_{et}^b	Base-case power flow of line l and phase angle of power bus e at time t .
S_{it}^{gas}	Binary indicator which is 1 if unit i switches
	from gas to traditional fuel at time t , and otherwise 0 .
S_{it}^{fuel}	Binary indicator which is 1 if unit i switches from traditional fuel to gas at time t , and otherwise 0.
$SU_{it}^{\rm gas}$, $SD_{it}^{\rm gas}$	Startup/shutdown cost of unit i at time t when burning gas fuel.
SU_{it}^{fuel} , SD_{it}^{fuel}	Startup/shutdown cost of unit i at time t when burning traditional fuel.
v_{dt}	Load shedding of power load d at time t .
v_{gt}	Load shedding of gas load g at time t .
1)	W' 1 - '11 C' 1 C 4 ' 4
v_{wt}	Wind spillage of wind farm w at time t.
v_{wt} $X_{it}^{\text{on}}, X_{it}^{\text{off}}$	Wind spillage of wind farm w at time t . ON/OFF time counter of unit i at time t .
X_{it}^{on} , X_{it}^{off}	ON/OFF time counter of unit i at time t .
X_{it}^{on} , X_{it}^{off} δ_{dt}^{\pm} , δ_{wt}^{\pm} , δ_{gt}^{\pm}	ON/OFF time counter of unit i at time t . Binary indicators describing uncertainty sets. Base-case pressure of gas node m at time t . Variables corresponding to uncertainties/worst
$X_{it}^{\text{on}}, X_{it}^{\text{off}}$ $\delta_{dt}^{\pm}, \delta_{wt}^{\pm}, \delta_{gt}^{\pm}$ π_{mt}^{b} $(\cdot)^{u}, (\cdot)^{wc}$	ON/OFF time counter of unit i at time t . Binary indicators describing uncertainty sets. Base-case pressure of gas node m at time t .
$X_{it}^{\text{on}}, X_{it}^{\text{off}}$ $\delta_{dt}^{\pm}, \delta_{wt}^{\pm}, \delta_{gt}^{\pm}$ π_{mt}^{b} $(\cdot)^{u}, (\cdot)^{wc}$ E. Constants:	ON/OFF time counter of unit i at time t . Binary indicators describing uncertainty sets. Base-case pressure of gas node m at time t . Variables corresponding to uncertainties/worst
$X_{it}^{\text{on}}, X_{it}^{\text{off}}$ $\delta_{dt}^{\pm}, \delta_{wt}^{\pm}, \delta_{gt}^{\pm}$ π_{mt}^{b} $(\cdot)^{u}, (\cdot)^{wc}$ E. Constants: $c_{ih}^{\text{gas}}, c_{ih}^{\text{fuel}}$	ON/OFF time counter of unit i at time t . Binary indicators describing uncertainty sets. Base-case pressure of gas node m at time t . Variables corresponding to uncertainties/worst
$X_{it}^{\text{on}}, X_{it}^{\text{off}}$ $\delta_{dt}^{\pm}, \delta_{wt}^{\pm}, \delta_{gt}^{\pm}$ π_{mt}^{b} $(\cdot)^{u}, (\cdot)^{wc}$ E. Constants:	ON/OFF time counter of unit i at time t . Binary indicators describing uncertainty sets. Base-case pressure of gas node m at time t . Variables corresponding to uncertainties/worst cases. Incremental fuel consumption of unit i at
$X_{it}^{\text{on}}, X_{it}^{\text{off}}$ $\delta_{dt}^{\pm}, \delta_{wt}^{\pm}, \delta_{gt}^{\pm}$ π_{mt}^{b} $(\cdot)^{u}, (\cdot)^{wc}$ E. Constants: $c_{ih}^{\text{gas}}, c_{ih}^{\text{fuel}}$	ON/OFF time counter of unit i at time t . Binary indicators describing uncertainty sets. Base-case pressure of gas node m at time t . Variables corresponding to uncertainties/worst cases. Incremental fuel consumption of unit i at segment h when burning gas/traditional fuel.
$X_{it}^{\text{on}}, X_{it}^{\text{off}}$ $\delta_{dt}^{\pm}, \delta_{wt}^{\pm}, \delta_{gt}^{\pm}$ π_{mt}^{b} $(\cdot)^{u}, (\cdot)^{wc}$ E. Constants: $c_{ih}^{\text{gas}}, c_{ih}^{\text{fuel}}$	ON/OFF time counter of unit <i>i</i> at time <i>t</i> . Binary indicators describing uncertainty sets. Base-case pressure of gas node <i>m</i> at time <i>t</i> . Variables corresponding to uncertainties/worst cases. Incremental fuel consumption of unit <i>i</i> at segment <i>h</i> when burning gas/traditional fuel. Price of traditional fuel for unit <i>i</i> .
$X_{it}^{\text{on}}, X_{it}^{\text{off}}$ $\delta_{dt}^{\pm}, \delta_{wt}^{\pm}, \delta_{gt}^{\pm}$ π_{mt}^{b} $(\cdot)^{u}, (\cdot)^{wc}$ E. Constants: $c_{ih}^{\text{gas}}, c_{ih}^{\text{fuel}}$ C_{i}^{fuel}	ON/OFF time counter of unit <i>i</i> at time <i>t</i> . Binary indicators describing uncertainty sets. Base-case pressure of gas node <i>m</i> at time <i>t</i> . Variables corresponding to uncertainties/worst cases. Incremental fuel consumption of unit <i>i</i> at segment <i>h</i> when burning gas/traditional fuel. Price of traditional fuel for unit <i>i</i> . Production cost of gas well <i>j</i> .
$X_{it}^{\text{on}}, X_{it}^{\text{off}}$ $\delta_{dt}^{\pm}, \delta_{wt}^{\pm}, \delta_{gt}^{\pm}$ π_{mt}^{b} $(\cdot)^{u}, (\cdot)^{wc}$ E. Constants: $c_{ih}^{\text{gas}}, c_{ih}^{\text{fuel}}$ C_{i}^{fuel} C_{j} C_{s} $C_{d}^{\text{ls}}, C_{w}^{\text{ws}}, C_{g}^{\text{gs}}$	ON/OFF time counter of unit <i>i</i> at time <i>t</i> . Binary indicators describing uncertainty sets. Base-case pressure of gas node <i>m</i> at time <i>t</i> . Variables corresponding to uncertainties/worst cases. Incremental fuel consumption of unit <i>i</i> at segment <i>h</i> when burning gas/traditional fuel. Price of traditional fuel for unit <i>i</i> . Production cost of gas well <i>j</i> . Operation cost of gas storage facility <i>s</i> . Costs of power load shedding, wind spillage, and gas load shedding.
$X_{it}^{\text{on}}, X_{it}^{\text{off}}$ $\delta_{dt}^{\pm}, \delta_{wt}^{\pm}, \delta_{gt}^{\pm}$ π_{mt}^{b} $(\cdot)^{u}, (\cdot)^{wc}$ E. Constants: $c_{ih}^{\text{gas}}, c_{ih}^{\text{fuel}}$ C_{i}^{fuel} C_{j} C_{s} $C_{d}^{\text{ls}}, C_{w}^{\text{ws}}, C_{g}^{\text{gs}}$	ON/OFF time counter of unit <i>i</i> at time <i>t</i> . Binary indicators describing uncertainty sets. Base-case pressure of gas node <i>m</i> at time <i>t</i> . Variables corresponding to uncertainties/worst cases. Incremental fuel consumption of unit <i>i</i> at segment <i>h</i> when burning gas/traditional fuel. Price of traditional fuel for unit <i>i</i> . Production cost of gas well <i>j</i> . Operation cost of gas storage facility <i>s</i> . Costs of power load shedding, wind spillage,
$X_{it}^{\text{on}}, X_{it}^{\text{off}}$ $\delta_{dt}^{\pm}, \delta_{wt}^{\pm}, \delta_{gt}^{\pm}$ π_{mt}^{b} $(\cdot)^{u}, (\cdot)^{wc}$ E. Constants: $c_{ih}^{\text{gas}}, c_{ih}^{\text{fuel}}$ C_{i}^{fuel} C_{j} C_{s} $C_{d}^{\text{ls}}, C_{w}^{\text{ws}}, C_{g}^{\text{gs}}$ $K_{p}^{\text{gf}}, K_{p}^{\text{lp}}$ M	ON/OFF time counter of unit <i>i</i> at time <i>t</i> . Binary indicators describing uncertainty sets. Base-case pressure of gas node <i>m</i> at time <i>t</i> . Variables corresponding to uncertainties/worst cases. Incremental fuel consumption of unit <i>i</i> at segment <i>h</i> when burning gas/traditional fuel. Price of traditional fuel for unit <i>i</i> . Production cost of gas well <i>j</i> . Operation cost of gas storage facility <i>s</i> . Costs of power load shedding, wind spillage, and gas load shedding.

of wind farm w/gas load g at time t. $\tilde{\Gamma}$, $\tilde{\Gamma}$, \tilde{C} Uncertainty deviation of power load d/wind farm w/gas load g at time t. R_i^{up} , R_i^{down} Up/down corrective action limit of unit i. $su_i^{\rm gas}$, $sd_i^{\rm gas}$ Startup/shutdown cost of unit i when burning su_i^{fuel} , sd_i^{fuel} Startup/shutdown cost of unit i when burning traditional fuel. S_i^{\max} Maximum fuel switching limit of unit i. SR_t System spinning reserve requirement at time t. $T_i^{\text{on}}, T_i^{\text{off}}$ Minimum ON/OFF time limit of unit *i*. Ramp up/down rate limit of unit i. UR_i , DR_i vmax Predefined threshold on monetary system security violation, in terms of total penalty cost of power load shedding, wind spillage, and gas load shedding. Compressor factor of active pipelines p. Efficiency of PtG facility a. Fuel consumption factor of active pipeline p. Budget of uncertainty for power loads/wind Δ_d , Δ_w , Δ_g generations/gas loads.

1. Introduction

 $(\cdot)^{\min/\max}$

Thanks to the sharp decrease in natural gas price and the distinct advantages of gas-fired generators including smaller capital cost, higher efficiency, faster response capability, and lower carbon emission, natural gas is becoming the top choice of fuel for building new generators in electric power systems [1]. Furthermore, power-to-gas (PtG) as a new promising technology could effectively convert excessive renewable energy into compatible natural gas [2]. The impact of PtG on electrical and gas transmission networks is studied in [3]. As a result, the power system relies more on the natural gas system in terms of supplying and delivering gas fuel to gas-fired units and utilizing gas produced from PtGs. On the other hand, electric-driven gas compressors, which could compensate pressure losses in the gas network, rely on electricity supply from the power grid.

Min/max value of a quantity.

In this regard, the electric power system and the natural gas system are interdependent with each other, e.g., the secure and economic operation of one energy system would directly impact and be influenced by that of the other [4]. Indeed, gas supply shortage of the gas network could lead to forced outage of multiple gas-fired units, while power transmission line security violations could result in shutdown of multiple gas compressor stations. Both situations would greatly jeopardize security of the two energy systems [5]. In turn, considering the

interdependency of power and gas systems, co-optimizing them as a whole integrated system (e.g., the IPGS) could achieve a more secure and economic operation of both systems.

Focusing on enhancing secure and economic operation of IPGS, coordinated day-ahead scheduling of power system and gas system has been studied in several literature [6]-[10] under the deterministic setting. A short-term security-constrained UC is developed in [6] while considering the impact of natural gas transmission network constraints. Reference [7] aims on an integrated formulation to analyze steady-state electricity and natural gas systems. A novel MILP formulation of an integrated power and natural gas system is proposed in [8] while taking into account gas traveling velocity and compressibility. A unified energy flow formulation is presented in [9] to describe the bi-directional energy conversion in an integrated natural gas and electric power system. Reference [10] proposes a bi-level economic dispatch model for the integrated natural gas and electricity system, in which the upper level is an economical dispatch problem of the electricity system and the lower level is an optimal allocation problem of the natural gas network.

As uncertainties of power loads, renewable energy (wind generation in particular), and gas loads bring additional challenges for managing operational security of the IPGS, coordinated operation of IPGS with respect to major power system uncertainties is further studied in literature [11]-[17]. Reference [11] presents a mid-term stochastic securityconstrained model for optimally coordinating water and natural gas supplies to power systems while considering random outages of power system components, electricity load forecast errors, and water inflow fluctuations. Reference [12] utilizes quick-ramping capabilities of gas-fired units to compensate variability and uncertainty of wind generation, while minimizing total operation cost of the power grid with respect to both electricity grid and gas network constraints. Reference [13] studies a stochastic day-ahead electric power system scheduling model while considering natural gas transmission constraints, random outages of generating units/transmission lines, and forecasting errors of electric power loads. Reference [14] formulates a two-stage stochastic optimization problem to determine the short-term energy and reserve schedule while considering electricity demand response. Two interval algorithm-based models are presented in [15] to study the impact of wind power output uncertainty on coupled natural gas and electricity networks. Robust optimization-based models are also proposed in [16]-[17] to explore coordinated scheduling of electricity and natural gas systems. Specifically, reference [16] focuses on distributed computation of electricity and natural gas systems which could keep information privacy of the two systems, while [17] discusses the effectiveness of PtG facilities for handling wind generation uncertainties.

Indeed, above review on existing literature indicates several key shortcomings that need to be adequately addressed: 1) Although robust optimization has been used to study impacts of power system uncertainties on operational security and economics of IPGS [16]-[17], influence of gas system uncertainties, fluctuating natural gas demands in particular, has not been studied under any robust optimization framework,

which is mainly because of additional computational challenges introduced by nonlinear gas flow equations. Indeed, because residential gas loads have higher priorities than gas-fired units, a sharp increase in residential gas demands, especially in cold winter days, could potentially cause gas supply deficit to gas-fired units and comprise power system security. Consequently, natural gas demand uncertainties could significantly impact operational security of the IPGS and should be adequately addressed in the IPGS operation scheduling framework. 2) Benefits of other advanced technologies, such as dual-fuel units that could help shave peak gas demands and maintain operational security and economy of IPGS under uncertainties, have not been explored sufficiently.

This paper proposes an adjustable robust day-ahead scheduling model for the IPGS, while simultaneously considering uncertainties of the power system (e.g., power loads and renewable energy) and the gas system (e.g., gas loads). Furthermore, dual-fuel units are considered as an effective mean to shave peak gas demands and maintain the secure and economic operation of IPGS during peak gas demand hours [5], [18]. In addition, it is well understood that MILP based piecewise linear approximations of Weymouth gas flow equations [8], [12], [16] significantly complicate the calculation of robust optimization models, because binary variables in gas flow approximation models prevent dualizing lower-level economic dispatch problem in the second-stage subproblem. In order to effectively solve the proposed adjustable robust optimization model, Taylor series expansion is adopted in this paper to approximate nonlinear Weymouth gas flow constraints via a set of linear constraints.

Major contributions of this paper are threefold.

- 1) Interdependency Modeling: The IPGS is rigorously modeled by considering key coupling components of the two systems, including gas-fired units, dual-fuel units, PtG facilities, and electric-driven compressors. Specifically, gas-fired units and dual-fuel units rely on the gas network for gas fuel supply, while electric-driven compressors and PtG facilities depend on the power grid for electricity supply.
- 2) Uncertainty Consideration: A two-stage adjustable robust model is proposed to derive physically secure and economically viable solutions, for optimally operating IPGS against various uncertainties of power loads, wind generations, and gas loads. Specifically, the proposed adjustable robust model minimizes total cost in base case, while maintaining operational security against all possible situations within predefined uncertainty sets.
- 3) Nonlinear Gas Flow Equation Approximation: Bi-directional nonlinear gas flow equations are represented as an MILP formulation via Taylor series expansion, in which only a limited number of binary variables is needed to identify gas flow directions. Thus, after gas flow directions are determined in the master problem, the max-min security checking sub-problem can be recast into a single-level maximization problem via duality theory, because the inner-level minimization problem becomes an LP model. In this way, the proposed two-stage adjustable robust model can be efficiently solved via CCG [16], [19].

The remainder of the paper is as follows. Sections 2 and 3 describe the adjustable robust scheduling model and the solution methodology. Numerical case studies are presented in Section 4, and conclusions are given in Section 5.

2. Robust Formulations of IPGS

This section first provides an overview of IPGS, in which the electric power system and the natural gas system are coupled through gas-fired units, dual-fuel units, PtG facilities, and electric-driven compressors. Next, the adjustable robust optimization-based day-ahead coordinated scheduling model is presented with respect to base-case operation and uncertainty situations.

2.1 Overview of IPGS

Interactions between electric power system and natural gas system are highlighted in Fig. 1, in which gas-fired units (including dual-fuel units), PtG facilities, and electric-driven compressors represent linkages between the two systems. Specifically, in an IPGS, the electric power system relies on the natural gas network for supplying gas fuel to gas-fired/dual-fuel units and absorbing natural gas converted by PtG facilities; While the natural gas system relies on the electric power system to operate electric-driven gas compressors for facilitating natural gas transportation. Indeed, under highly interdependent circumstance, the economic and secure operation of one energy system would directly impact and be influenced by that of the other. Specifically:

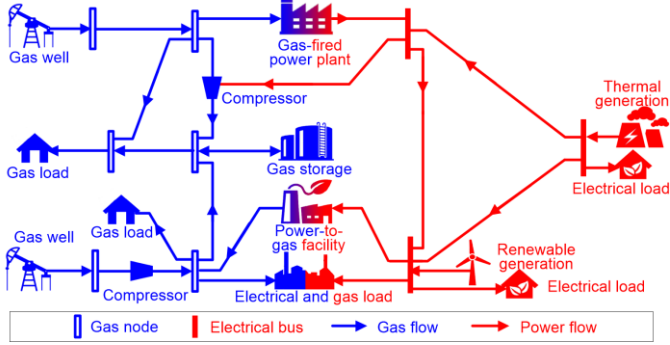


Fig. 1. Interaction between electric power system and natural gas system.

- Interdependency in Economic Operation: Because of the limited gas transmission capacity and a higher priority of residential gas loads, gas fuel unavailability of gas-fired units could significantly increase operation cost of power system by turning on more expensive power plants. On the other hand, because dispatches of gas-fired units are frequently adjusted more often to offset variations of electrical loads and renewable generations, natural gas system operators are facing with more significant gas load volatility with increased operation cost of the natural gas system.
- Interdependency in Secure Operation: Gas supplier shortages and gas pipeline congestions could lead to forced outage of multiple gas-fired units; While electric transmission line congestion could result in shutdown of multiple electric-driven compressor stations.

Consequently, in this paper, electric power system and

natural gas system are modeled as a whole integrated system under the robust optimization framework to ensure its economic and secure operations.

2.2 Robust Formulations

This paper proposes a two-stage adjustable robust model to study day-ahead coordinated optimal scheduling of the IPGS. Specifically, the IPGS is designed to operate under base-case conditions with respect to forecast values of power loads, wind generation, and gas loads in the day-ahead timeframe, while it can adaptively and securely redispatch generating units, gas wells, and gas compressors when uncertainties are revealed in real time [20]-[22]. This operation scheme perfectly fits the concept of two-stage adjustable robust model. That is, the first stage determines unit commitment statuses of generators, fuel types of dual-fuel units, and gas flow directions of gas pipelines in the base-case scenario, while the second stage finds redispatches when uncertainties are revealed.

The following assumptions are adopted in the proposed two-stage adjustable robust scheduling model.

- 1) Unit commitment statuses are the first stage variables, i.e., they remain fixed when uncertainties are revealed [16], [20], [21]. This is recognized by the fact that physical characteristics of most generating units restrict them from quickly changing their unit commitment statuses under uncertainties.
- 2) Dual-fuel units cannot switch fuel type in response to uncertainties, as it could take up to hours for them to switch from one fuel to another [23]-[24].
- 3) Gas flow direction of an inactive pipeline cannot be reversed when uncertainties are revealed. It is pointed out in [25] that reversing gas flows may lead to complicated changes in operation statuses of multiple facilities such as overpressure protection devices, control valves, and compressor stations. Thus, reversing gas flow directions is only allowed in the first stage with sufficient time and appropriate management.
- 4) All compressors are electric-driven with linear cost functions [26]-[27]. According to [27], typical energy consumption of compressor stations is equivalent to about 3-5% of total transported gas quantity.

The proposed two-stage adjustable robust scheduling model is described below in details.

2.2.1 Objective Function

The objective of the proposed two-stage adjustable robust co-optimization scheduling model is to minimize base-case total costs of the IPGS for supplying power and gas loads. In Equation (1), the three terms represent operation cost of non-gas-fired units, production cost of natural gas wells to supply gas loads (including gas-fired and dual-fuel units), and operation cost of gas storage facilities for storing gas in and withdrawing gas out of them.

$$\min \sum_{t} \left[\sum_{i \in \mathbf{DF} \cup \mathbf{TU}} C_i^{\text{fuel}} \cdot F_{it}^{b, \text{fuel}} + \sum_{j} C_j \cdot G_{jt}^{b} + \sum_{s} C_s \cdot G_{st}^{b, \text{in}} \right]$$
(1)

2.2.2 Base-Case Constraints

Base-case constraints of the IPGS include those for

individual electric power and natural gas systems, as well as coupling constraints that describe interdependency of the two systems.

• Base-Case Power System Constraints

Base-case power system constraints are presented as in (2)-(6). Specifically, constraint (2a) represents system spinning reserve requirement. Individual generators need to satisfy minimum ON/OFF time limits (2b)-(2c). Equation (2d) indicates that regular generating units and PtG facilities connected at the same bus will not operate simultaneously.

$$\sum_{i} P_{i}^{\text{max}} \cdot I_{it} \ge \sum_{d} P_{dt}^{b} + SR_{t} \tag{2a}$$

$$\left(X_{i(t-1)}^{\text{on}} - T_i^{\text{on}}\right) \left(I_{i(t-1)} - I_{it}\right) \ge 0$$
 (2b)

$$\left(X_{i(t-1)}^{\text{off}} - T_i^{\text{off}}\right) \left(I_{it} - I_{i(t-1)}\right) \ge 0 \tag{2c}$$

$$I_{it} + I_{at} \le 1, \quad \forall i, a \in N(e)$$
 (2d)

Other base-case power system operation constraints include system load balance (3a), DC power flow equations (3b)-(3d), ramp up and down limits (3e)-(3f), as well as capacity limits of generating units (3g) and PtG facilities (3h). It is worth mentioning that electric-driven compressors are considered in

(3a) as power loads P_{pt}^b in the power grid.

$$\sum_{i \in N(e)} P_{it}^{b} + \sum_{w \in N(e)} P_{wt}^{b} - \sum_{s(l) \in N(e)} P_{lt}^{b} + \sum_{r(l) \in N(e)} P_{lt}^{b}$$

$$- \sum_{a \in N(e)} P_{at}^{b} = \sum_{d \in N(e)} P_{dt}^{b} + \sum_{p \in N(e) \cap} P_{pt}^{b}$$
(3a)

$$P_{lt}^b = \left(\theta_{s(l)t}^b - \theta_{r(l)t}^b\right) / x_l \tag{3b}$$

$$-P_l^{\max} \le P_{lt}^b \le P_l^{\max} \tag{3c}$$

$$\theta_e^{\min} \le \theta_{et}^b \le \theta_e^{\max} \tag{3d}$$

$$P_{it}^{b} - P_{i(t-1)}^{b} \le UR_i \cdot I_{i(t-1)} + P_i^{\min} \cdot (I_{it} - I_{i(t-1)}) + P_i^{\max} \cdot (1 - I_{it})$$
(3e)

$$P_{i(t-1)}^{b} - P_{it}^{b} \le DR_{i} \cdot I_{it} + P_{i}^{\min} \cdot (I_{i(t-1)} - I_{it}) + P_{i}^{\max} \cdot (1 - I_{i(t-1)})$$
(3f)

$$P_i^{\min} \cdot I_{it} \le P_{it}^b \le P_i^{\max} \cdot I_{it}$$
 (3g)

$$0 \le P_{at}^b \le P_a^{\text{max}} \cdot I_{at} \tag{3h}$$

Fuel consumption and fuel-switching limit of dual-fuel units are modeled as in (4)-(6). Constraint (4a) describes that a fuel-switching unit either burns natural gas or traditional fuel. Startup/shutdown costs when burning natural gas or traditional fuel are shown in (4b)-(4e). Constraint (5) calculates total fuel consumptions of individual dual-fuel units. In addition, dual-fuel units can only switch between natural gas and traditional fuel for a limited number of times throughout a day (6a), while fuel-switching logic constraints are restricted via (6b)-(6f). Fuel consumptions of traditional units and gas-fired units can be similarly described as those in (4)-(5).

$$I_{it} = I_{it}^{\text{gas}} + I_{it}^{\text{fuel}}, i \in \mathbf{DF}$$
 (4a)

$$SU_{it}^{\text{gas}} \ge su_i^{\text{gas}} \cdot \left(I_{it}^{\text{gas}} - I_{i(t-1)}^{\text{gas}}\right), SU_{it}^{\text{gas}} \ge 0, i \in \mathbf{DF}$$
 (4b)

$$SD_{it}^{\text{gas}} \ge sd_i^{\text{gas}} \cdot \left(I_{i(t-1)}^{\text{gas}} - I_{it}^{\text{gas}}\right), SD_{it}^{\text{gas}} \ge 0, i \in \mathbf{DF}$$
 (4c)

$$SU_{it}^{\text{fuel}} \ge su_i^{\text{fuel}} \cdot \left(I_{it}^{\text{fuel}} - I_{i(t-1)}^{\text{fuel}}\right), SU_{it}^{\text{fuel}} \ge 0, i \in \textbf{\textit{DF}} \tag{4d}$$

$$SD_{it}^{\text{fuel}} \ge sd_i^{\text{fuel}} \cdot \left(I_{i(t-1)}^{\text{fuel}} - I_{it}^{\text{fuel}}\right), SD_{it}^{\text{fuel}} \ge 0, i \in \mathbf{DF}$$
 (4e)

$$0 \le P_{iht}^{b,\text{gas}} \le P_{ih}^{\text{max}} \cdot I_{it}^{\text{gas}}, i \in \mathbf{DF}$$
 (5a)

$$0 \le P_{iht}^{b,\text{fuel}} \le P_{ih}^{\text{max}} \cdot I_{it}^{\text{fuel}}, i \in \mathbf{DF}$$
 (5b)

$$P_{it}^b = P_i^{\rm gas,\,min} \cdot I_{it}^{\rm gas} + \sum\limits_h P_{iht}^{b,\rm gas} + P_i^{\rm fuel,\,min} \cdot I_{it}^{\rm fuel} + \sum\limits_h P_{iht}^{b,\rm fuel},$$

 $i \in \mathbf{DF}$ (5c)

$$F_{it}^{b,\mathrm{gas}} = F_{it}^{\mathrm{gas,min}} \cdot I_{it}^{\mathrm{gas}} + \sum_{h} c_{ih}^{\mathrm{gas}} \cdot P_{iht}^{b,\mathrm{gas}} + SU_{it}^{\mathrm{gas}} + SD_{it}^{\mathrm{gas}},$$

 $i \in \mathbf{DF}$ (5d)

$$F_{it}^{b,\mathrm{fuel}} = F_{it}^{\mathrm{fuel,min}} \cdot I_{it}^{\mathrm{fuel}} + \sum_{h} c_{ih}^{\mathrm{fuel}} \cdot P_{iht}^{b,\mathrm{fuel}} + SU_{it}^{\mathrm{fuel}} + SD_{it}^{\mathrm{fuel}} \,,$$

 $i \in \mathbf{DF}$ (5e)

$$\sum_{t} \left(S_{it}^{\text{gas}} + S_{it}^{\text{fuel}} \right) \le S_{i}^{\text{max}}, i \in \mathbf{DF}$$
 (6a)

$$S_{it}^{\text{gas}} + S_{it}^{\text{fuel}} \le I_{it}, i \in \mathbf{DF}$$
 (6b)

$$S_{it}^{\text{gas}} \le I_{i(t-1)}^{\text{gas}}, i \in \mathbf{DF}$$
 (6c)

$$S_{it}^{\text{gas}} \ge I_{i(t-1)}^{\text{gas}} - I_{it}^{\text{gas}}, i \in \mathbf{DF}$$

$$\tag{6d}$$

$$S_{it}^{\text{fuel}} \le I_{i(t-1)}^{\text{fuel}}, i \in \mathbf{DF}$$
 (6e)

$$S_{it}^{\text{fuel}} \ge I_{i(t-1)}^{\text{fuel}} - I_{it}^{\text{fuel}}, i \in \mathbf{DF}$$
 (6f)

• Base-Case Natural Gas System Constraints

Base-case natural gas system constraints are presented as in (7)-(11). Gas network nodal balance equation (7a) represents that total gas flow injection is equal to total gas withdrawn at each gas node. Nodal pressures and production capabilities of gas wells are limited in (7b) and (7c), respectively.

$$\begin{split} & \sum_{j \in G(m)} G^{b}_{jt} - \sum_{s(p) \in G(m)} G^{b,\text{in}}_{pt} + \sum_{r(p) \in G(m)} G^{b,\text{out}}_{pt} + \sum_{a \in G(m)} G^{b}_{at} \\ & + \sum_{s \in G(m)} \left(G^{b,\text{out}}_{st} - G^{b,\text{in}}_{st} \right) = \sum_{i \in G(m)} G^{b}_{it} + \sum_{g \in G(m)} G^{b}_{gt} \quad (7a) \end{split}$$

$$\pi_m^{\min} \le \pi_m^b \le \pi_m^{\max} \tag{7b}$$

$$G_i^{\min} \le G_{it}^b \le G_i^{\max} \tag{7c}$$

Equations (8)-(9) describe dynamic network operation characteristics of inactive pipelines with varying incoming and outgoing gas flows. Specifically, (8a) is Weymouth gas flow equation of inactive pipelines [28]-[30], where average gas flow is calculated via (8b). Gas flow directions of inactive

pipelines are determined by (8c)-(8f), where $f_{pt}^+=1$ indicates that gas flow is in positive direction, i.e., pressure of the sending node is higher than the receiving node. In addition, linepack represents the quantity of natural gas contained in an inactive pipeline, which can be used to handle variations in gas demands that may not be balanced instantaneously by gas production wells [31]. Linepack of an inactive pipeline is proportional to average nodal pressure (9a)-(9b) and time-coupled with all previous pipeline inflows/outflows (9c) [8], [16].

$$\tilde{C}_{\perp} = -f_{pt}^{-} \cdot K_{p}^{\text{gf}} \cdot \sqrt{\left(\pi_{s(p)t}^{b}\right)^{2} - \left(\pi_{r(p)t}^{b}\right)^{2}}, p \in \Omega_{P} \quad (8a)$$

$$\tilde{C}$$
 $\lim_{t \to \infty} + G_{pt}^{b,\text{out}} / 2, p \in \Omega_P$ (8b)

$$-\left(1-f_{pt}^{+}\right)\cdot M \le \pi_{s(p)t}^{b} - \pi_{r(p)t}^{b} \le \left(1-f_{pt}^{-}\right)\cdot M, p \in \Omega_{P} \quad (8c)$$

$$-\left(1-f_{pt}^{+}\right)\cdot M \leq G_{pt}^{b,\text{in}} \leq \left(1-f_{pt}^{-}\right)\cdot M, p \in \Omega_{P} \tag{8d}$$

$$-\left(1-f_{pt}^{+}\right)\cdot M \leq G_{pt}^{b,\text{out}} \leq \left(1-f_{pt}^{-}\right)\cdot M, p \in \Omega_{P} \tag{8e}$$

$$f_{pt}^{+} + f_{pt}^{-} = 1, p \in \Omega_{P}$$
 (8f)

$$E_{pt}^{b} = K_{p}^{lp} \cdot \tilde{r} \qquad \Omega_{P}$$
 (9a)

$$\tilde{s} \qquad \frac{b}{mt} + \pi \frac{b}{nt} \Big) \Big/ 2, p \in \Omega_P \tag{9b}$$

$$E_{pt}^{b} = E_{p(t-1)}^{b} + G_{pt}^{b,\text{in}} - G_{pt}^{b,\text{out}}, p \in \Omega_{P}$$
(9c)

An active gas pipeline equipped with a gas compressor usually has predefined gas flow direction (10a), and presents equal gas inflow and outflow (10b). In addition, terminal nodal pressures of active pipelines are constrained via compressor factor as in (10c) [32].

$$G_{pt}^{b,\text{in}} \ge 0, p \in \Omega_C \tag{10a}$$

$$G_{pt}^{b,\mathrm{in}} = G_{pt}^{b,\mathrm{out}}, p \in \Omega_C$$
 (10b)

$$\pi_{r(p)t}^{b} \le \Gamma_{p}^{\text{com}} \cdot \pi_{s(p)t}^{b}, p \in \Omega_{C}$$
(10c)

Operational characters of gas storage facilities are described as in (11), including gas storage balance (11a), storage capacity limit (11b), as well as lower/upper limits of storage inflow rates (11c) and storage outflow rates (11d).

$$E_{st}^{b} = E_{s(t-1)}^{b} + G_{st}^{b,\text{in}} - G_{st}^{b,\text{out}}$$
(11a)

$$E_s^{\min} \le E_{st}^b \le E_s^{\max} \tag{11b}$$

$$G_s^{\text{in,min}} \le G_{st}^{b,\text{in}} \le G_s^{\text{in,max}}$$
 (11c)

$$G_s^{\text{out,min}} \le G_{st}^{b,\text{out}} \le G_s^{\text{out,max}}$$
 (11d)

• Base-Case Coupling Constraints of the IPGS

In an IPGS, the power system relies on the gas system to supply gas fuel to gas-fired/dual-fuel units and to absorb gas converted from PtG facilities, while the gas system relies on the power system to power gas compressors for facilitating natural gas transportation. PtG contains two main processes of

electrolysis and methanization [2], [9], through which electricity is converted into hydrogen and further into methane. The efficiency of converting electricity into natural gas is normally in the region of 0.49-0.65.

Base-case coupling constraints of the IPGS are presented as in (12). Three types of couplings are considered, including (i) gas-fired and dual-fuel units which consume gas fuel from the gas system and generate electricity in the power system (12a); (ii) PtG facilities which consume electricity from the power system and deliver gas into the gas system (12b) [9], [33]; and (iii) electric-driven gas compressors which consume electricity from the power system and support gas transportation (12c) [16], [34]. In (12), HHV equals 1.026 MBtu/kcf, and the energy conversion factor χ equals 3.4 MBtu/MWh.

$$G_{it}^{b} = F_{it}^{b,\text{gas}} / \text{HHV}, i \in \mathbf{GU} \cup \mathbf{DF}$$
 (12a)

$$G_{at}^b = \chi \cdot P_{at}^b \cdot \eta_a^{\text{ptg}} / \text{HHV}$$
 (12b)

$$P_{pt}^{b} = G_{pt}^{b,\text{in}} \cdot \eta_{p}^{\text{com}} \cdot \text{HHV} / \chi, p \in \Omega_{C}$$
 (12c)

For the sake of discussion, power system operation constraints (3) and (5), natural gas system operation constraints (7)-(11), and coupling constraints (12) are rewritten in a compact form as in (13).

$$\mathbf{L}^{\text{pg}}\left(P_{it}^{b}, P_{at}^{b}, P_{wt}^{b}, P_{dt}^{b}, G_{gt}^{b}, G_{jt}^{b}, G_{st}^{b, \text{out}}, G_{st}^{b, \text{in}}\right) \le 0$$
(13)

2.2.3 Constraints for Handling Uncertainties

The proposed two-stage adjustable robust optimization model minimizes total cost in the base case while maintaining system security with respect to all possible uncertainty realizations within a predefined uncertainty set. The worst-case security violation under uncertainties is identified via a maximin calculation as in (14a), which is further limited by a predefined system security level $v^{\rm max}$ to ensure physically secure operation of IPGS. That is, the total penalty of electric load shedding, wind spillage, and gas load shedding should be no larger than $v^{\rm max}$ under any circumstance. Moreover, a higher priority of residential gas loads over gas-fired units is

reflected by a larger load shedding costs $C_g^{
m gs}$ over $C_d^{
m ls}$. That

is, a relatively larger gas load shedding cost $C_g^{\rm gs}$ of residential gas loads would drive that available gas will be first used to meet residential gas loads, instead of supplying gas-fired units to generate electricity. Constraints (14b)-(14e) describe uncertainty sets of power loads, wind generation, and gas loads [35]-[36]. Constraints (14f)-(14g) depict relaxed nodal power/gas balance requirements with additional slack valuables for power load shedding v_{dt} , wind spillage v_{wt} , and natural gas load shedding v_{gt} . Dispatch adjustments in response to uncertainty are limited by corrective ramp capabilities of generating units (14h). Constraint (14h) describes dispatch adjustment of generating units in response to uncertainties of electric load and wind generation. Up corrective capability

 R_i^{up} and down corrective capability R_i^{down} refer to the 10-min spinning reserve of generating units [16], [20]. In the day-ahead scheduling, the IPGS is designed to operate under the base-case scenario with unit commitment and dispatch decisions corresponding to the forecasted values of electric load, gas load, and wind generation, while dispatches could be adaptively and securely adjusted in real time. Specifically, generation dispatches of units are constrained by their corrective capabilities (14h). The compact form (14i) represents power system operation constraints, natural gas system operation constraints, and coupling constraints under uncertainties corresponding to base-case operation constraints (13). Boundaries of power load shedding, wind spillage, and gas load shedding are enforced by (14j)-(14l).

$$\max_{\left\{P_{dt}^{u}, P_{wt}^{u}, G_{gt}^{u}\right\}} \min_{\left\{v, P, \theta, \pi\right\}} \sum_{t} \left(\sum_{d} C_{d}^{ls} \cdot v_{dt} + \sum_{w} C_{w}^{ws} \cdot v_{wt} + \sum_{g} C_{g}^{gs} \cdot v_{gt}\right)$$

$$\leq v^{\text{max}}$$
 (14a)

$$\Omega_D = \begin{cases} P_{dt}^u \in \mathbb{R} & \sum\limits_{t} \left(\delta_{dt}^+ + \delta_{dt}^- \right) \leq \Delta_d, \delta_{dt}^+ + \delta_{dt}^- \leq 1 \\ P_{dt}^u = P_{dt}^b + \delta_{dt}^+ \cdot \tilde{i} & & \\ \vdots & & \vdots \\ \end{cases}$$

$$\Omega_{W} = \begin{cases} P_{wt}^{u} \in \mathbb{R} &: \sum_{t} \left(\delta_{wt}^{+} + \delta_{wt}^{-} \right) \leq \Delta_{w}, \delta_{wt}^{+} + \delta_{wt}^{-} \leq 1 \\ P_{wt}^{u} = P_{wt}^{b} + \delta_{wt}^{+} \cdot \tilde{I} & - \\ & & \\ & & \\ \end{cases}$$

$$\Omega_{G} = \begin{cases} G_{gt}^{u} \in \mathbb{R} & \sum_{t} \left(\delta_{gt}^{+} + \delta_{gt}^{-} \right) \leq \Delta_{g}, \delta_{gt}^{+} + \delta_{gt}^{-} \leq 1 \\ G_{gt}^{u} = G_{gt}^{b} + \delta_{gt}^{+} \cdot \tilde{C} & \sum_{d} \tilde{C}_{gt}^{-} \in \{0, 1\} \end{cases}$$

$$(14d)$$

$$P_{dt}^{u} \in \Omega_{D}, P_{wt}^{u} \in \Omega_{W}, G_{gt}^{u} \in \Omega_{G}$$

$$(14e)$$

$$\sum_{i \in N(e)} P_{it}^{u} + \sum_{w \in N(e)} \left(P_{wt}^{u} - v_{wt} \right) - \sum_{s(l) \in N(e)} P_{lt}^{u} + \sum_{r(l) \in N(e)} P_{lt}^{u}$$

$$- \sum_{a \in N(e)} P_{at}^{u} = \sum_{d \in N(e)} \left(P_{dt}^{u} - v_{dt} \right) + \sum_{p \in N(e) \cap} P_{pt}^{u} \quad (14f)$$

$$\begin{split} & \sum_{j \in G(m)} G^{u}_{jt} - \sum_{s(p) \in G(m)} G^{u,\text{in}}_{pt} + \sum_{r(p) \in G(m)} G^{u,\text{out}}_{pt} + \sum_{a \in G(m)} G^{u}_{at} \\ & + \sum_{s \in G(m)} \left(G^{u,\text{out}}_{st} - G^{u,\text{in}}_{st} \right) = \sum_{i \in G(m)} G^{u}_{it} + \sum_{g \in G(m)} \left(G^{u}_{gt} - v_{gt} \right) \end{split}$$

 $-R_i^{\text{down}} \cdot I_{it} \le P_{it}^u - P_{it}^b \le R_i^{\text{up}} \cdot I_{it}$ (14h)

$$\mathbf{L}^{\text{pg}}\left(P_{it}^{u}, P_{ot}^{u}, P_{wt}^{u}, P_{dt}^{u}, G_{ot}^{u}, G_{it}^{u}, G_{st}^{u, \text{out}}, G_{st}^{u, \text{in}}\right) \le 0 \tag{14i}$$

$$0 \le v_{dt} \le P_{dt}^u \tag{14j}$$

$$0 \le v_{wt} \le P_{wt}^u \tag{14k}$$

$$0 \le v_{\sigma t} \le G_{\sigma t}^u \tag{141}$$

3. Solution Methods

This section first discusses, based on the Taylor series expansion, how a bi-directional nonlinear Weymouth gas flow equation can be converted into an MILP formulation with only a few binary variables indicating gas flow directions. Then, a detailed CCG-based solution procedure is presented to effectively solve the proposed model. Specifically, with determined gas flow directions from the master problem, references [8] and [16] piecewisely linearize Weymouth gas flow equations with additional binary variables, which complicates the problem because duality theory cannot be directly applied to solve the maximin security evaluation subproblem; In comparison, the proposed Taylor series expansion based gas flow equation approximation could effectively avoid the introduction of additional binary variables and facilitate the calculation of CCG.

3.1 Linearize Weymouth Equations with Unknown Gas Flow Directions

This subsection first starts with Weymouth gas flow constraint (8a) for a gas pipeline operated in the positive flow direction (i.e., $f_{pt}^+=1$), which can be equivalently represented as in (15a). Applying the Taylor series expansion, linear approximation of (15a) around a pair of given terminal pressures $\left(\hat{\pi}_{s(p)t}^+, \hat{\pi}_{r(p)t}^+\right)$ (i.e., $\hat{\pi}_{s(p)t}^+ > \hat{\pi}_{r(p)t}^+$) is shown as in (15b) [32], [37].

$$\tilde{\zeta}$$
, $\sqrt{\left(\pi_{s(p)t}^b\right)^2 - \left(\pi_{r(p)t}^b\right)^2}$, $p \in \Omega_P$ (15a)

$$\tilde{\zeta} = \sqrt{\left(\hat{\pi}_{s(p)t}^{+}\right)^{2} - \left(\hat{\pi}_{r(p)t}^{+}\right)^{2}} + \frac{\partial \tilde{\zeta}}{\partial \pi_{s(p)t}^{b}} \left(\pi_{s(p)t}^{-} - \hat{\pi}_{s(p)t}^{+}\right)$$

$$+\frac{\partial \tilde{\ell}}{\partial \pi_{r(p)t}^{b}} \left(\pi_{r(p)t}^{\check{}} - \hat{\pi}_{r(p)t}^{+} \right), p \in \Omega_{P}$$
(15b)

By defining two sets of K breakpoints $\left(\hat{\pi}_{s(p)t,k}^+,\hat{\pi}_{r(p)t,k}^+\right)$

with $\hat{\pi}_{s(p)t,k}^+ \geq \hat{\pi}_{r(p)t,k}^+$ for k=1,2,...,K, K linear constraints in the form of (16a) represent an outer approximation of the cone described by the original Weymouth equation (15a), where $\phi_{pt,k}^+$ and $\phi_{pt,k}^+$ are defined as in (16b)-(16c).

$$\tilde{C} \qquad \varphi_{pt,k}^{+} \cdot \pi_{s(p)t}^{b} - K_{p}^{\text{gf}} \cdot \phi_{pt,k}^{+} \cdot \pi_{r(p)t}^{b},
p \in \Omega_{P} \text{ and } f_{pt}^{+} = 1$$
(16a)

$$\varphi_{pt,k}^{+} = \frac{\hat{\pi}_{s(p)t,k}^{+}}{\sqrt{\left(\hat{\pi}_{s(p)t,k}^{+}\right)^{2} - \left(\hat{\pi}_{r(p)t,k}^{+}\right)^{2}}}$$
(16b)

$$\phi_{pt,k}^{+} = \frac{\hat{\pi}_{r(p)t,k}^{+}}{\sqrt{\left(\hat{\pi}_{s(p)t,k}^{+}\right)^{2} - \left(\hat{\pi}_{r(p)t,k}^{+}\right)^{2}}}$$
(16c)

Similarly, for a gas pipeline operated in the negative gas flow direction (i.e., $f_{pt}^- = 1$), with another two sets of K breakpoints

$$\left(\hat{\pi}_{s(p)t,k}^{-},\hat{\pi}_{r(p)t,k}^{-}\right)$$
 with $\hat{\pi}_{s(p)t,k}^{-}<\hat{\pi}_{r(p)t,k}^{-}$ for $k=1,2,...,K,$

the Weymouth equation (8a) with negative gas flow direction can be linearized as in (17).

$$-\tilde{\zeta}, \qquad \varphi_{pt,k}^{-} \cdot \pi_{r(p)t}^{b} - K_{p}^{gf} \cdot \phi_{pt,k}^{-} \cdot \pi_{s(p)t}^{b},$$

$$p \in \Omega_{P} \text{ and } f_{pt}^{-} = 1$$

$$(17a)$$

$$\varphi_{pt,k}^{-} = \frac{\hat{\pi}_{r(p)t,k}^{-}}{\sqrt{\left(\hat{\pi}_{r(p)t,k}^{-}\right)^{2} - \left(\hat{\pi}_{s(p)t,k}^{-}\right)^{2}}}$$
(17b)

$$\phi_{pt,k}^{-} = \frac{\hat{\pi}_{s(p)t,k}^{-}}{\sqrt{\left(\hat{\pi}_{r(p)t,k}^{-}\right)^{2} - \left(\hat{\pi}_{s(p)t,k}^{-}\right)^{2}}}$$
(17c)

Finally, combining (16a) and (17a), Weymouth equation (8a) with unknown gas flow direction can be linearized as an MILP formulation (18).

$$\tilde{C}_{s} \cdot \varphi_{pt,k}^{+} \cdot \pi_{s(p)t}^{b} - K_{p}^{\text{gf}} \cdot \varphi_{pt,k}^{+} \cdot \pi_{r(p)t}^{b} + \left(1 - f_{pt}^{+}\right) \cdot M,$$

$$p \in \Omega_{P} \text{ (18a)}$$

$$-\tilde{C}_{s} \cdot \varphi_{pt,k}^{-} \cdot \pi_{r(p)t}^{b} - K_{p}^{\text{gf}} \cdot \varphi_{pt,k}^{-} \cdot \pi_{s(p)t}^{b} + \left(1 - f_{pt}^{-}\right) \cdot M,$$

$$p \in \Omega_{P} \text{ (18b)}$$

It is noteworthy that each pipeline is associated with 2K constraints (18a) and (18b), which altogether presents an outer approximation of the cone formed by the original Weymouth equation [32]. It is obvious that a larger value of K could derive a more accurate approximation. Indeed, at an optimal solution, only one that approximates gas flow most tightly will be binding.

3.2 Solution Algorithm

For the sake of discussion, the proposed two-stage adjustable robust optimization problem with linearized gas flow equations (18) is rewritten in a compact form as in (19).

$$\min_{(x,y)\in F(x,y)} c_b^{\mathsf{T}} x + c_g^{\mathsf{T}} y \tag{19a}$$

s.t.
$$Ax + By \le b$$
 (19b)

where
$$F(x, y) = \begin{cases} (x, y) : \max \min_{u = z, v} f^{T}v \le v^{\max} \\ \text{s.t. } Cx + Dy + Ez + Gv + Hu \le h \end{cases}$$
 (19c)

In (19), x represents binary variables related to unit commitment statuses of generators and gas flow directions of pipelines; y and z represent base-case continuous variables and corresponding adaptively adjusted variables under uncertainties; u is uncertain variables of power loads, wind generation, and gas loads described in (14b)-(14d); v represents vectors of power load shedding, wind spillage, and gas load shedding; A, B, C, D, E, G, and H are constant coefficient matrices, and c_b , c_g , b, f, and h are constant coefficient vectors, which all can be derived from (1)-(18).

In this paper, CCG is employed to solve the proposed two-stage adjustable robust optimization problem (19) in a master-subproblem framework.

• Master Problem

The master problem is presented as in (20), which minimizes base-case operation cost (20a), subject to base-case constraints (20b) and constraints (20c)-(20d) corresponding to individual worst-case realizations \boldsymbol{u}_q^* identified by the subproblem in all previous iterations.

$$\min_{\boldsymbol{x}, \boldsymbol{y}, \boldsymbol{z}_q, \boldsymbol{v}_q} \boldsymbol{c}_{\boldsymbol{b}}^{\mathrm{T}} \boldsymbol{x} + \boldsymbol{c}_{\boldsymbol{g}}^{\mathrm{T}} \boldsymbol{y} \tag{20a}$$

s.t.
$$Ax + By \le b$$
 (20b)

$$f^{\mathrm{T}} \mathbf{v}_{q} \le v^{\mathrm{max}}, \forall q \le n$$
 (20c)

$$Cx + Dy + Ez_q + Gv_q \le h - Hu_q^*, \forall q \le n$$
 (20d)

Solutions of unit commitment statuses and base-case dispatch of generators as well as gas flow directions of pipelines calculated from the master problem (20) will be passed onto the subproblem.

• Max-Min Subproblem

With given x^* and y^* from the master problem, the bi-level max-min subproblem (21) is calculated to identify the worst-case scenario that would lead to the largest possible system security violation. λ in the bracket is dual variable vector of the inner-level LP economic dispatch problem. The bi-level max-min subproblem (21) can be recast into a single-level equivalent bilinear maximization problem (22) by applying duality theory to the inner LP problem.

$$\max_{\mathbf{v}} \min_{\mathbf{z}, \mathbf{v}} \mathbf{f}^{\mathrm{T}} \mathbf{v} \tag{21a}$$

s.t.
$$Ez + Gv + Hu \le h - Cx^* - Dy^* : (\lambda)$$
 (21b)

$$\max_{\boldsymbol{u},\boldsymbol{\lambda}} \boldsymbol{\lambda}^{\mathrm{T}} \left(\boldsymbol{h} - \boldsymbol{C} \boldsymbol{x}^* - \boldsymbol{D} \boldsymbol{y}^* - \boldsymbol{H} \boldsymbol{u} \right) \tag{22a}$$

s.t.
$$\lambda^{\mathrm{T}} \mathbf{G} \leq \mathbf{f}$$
 (22b)

$$\boldsymbol{\lambda}^{\mathrm{T}}\boldsymbol{E} \leq \mathbf{0} \tag{22c}$$

$$l \le 0$$
 (22d)

Objective function (22a) includes bilinear terms, i.e. $\lambda^T u$. Because an uncertainty variable only takes forecast value or its upper/lower limit as indicated in (14b)-(14d), a bilinear term λu can be linearized as in (23).

$$\lambda u = \lambda^0 u^b + \lambda^+ u^+ + \lambda^- u^- \tag{23a}$$

$$\lambda = \lambda^0 + \lambda^+ + \lambda^- \tag{23b}$$

$$\beta^0 + \beta^+ + \beta^- = 1 \tag{23c}$$

$$-\beta^0 M \le \lambda^0 \le \beta^0 M \tag{23d}$$

$$-\beta^+ M \le \lambda^+ \le \beta^+ M \tag{23e}$$

$$-\beta^{-}M \le \lambda^{-} \le \beta^{-}M \tag{23f}$$

In (23), $\lambda^0/\lambda^+/\lambda^-$ and $\beta^0/\beta^+/\beta^-$ are auxiliary continuous and binary variables, corresponding to the situation when u takes the forecast value u^b /the upper bound u^+ /the lower bound u^- .

• The Detailed Solution Procedure of CCG

As shown in Fig. 2, the detailed implementation of CCG algorithm includes the following major steps:

Step 1: Initialize the system security violation threshold under uncertainties v^{max} and the iteration counter n=0.

Step 2: Solve the master problem (20), and pass optimal solutions x^* and y^* to the security checking subproblem (22).

Step 3: Solve the worst-case identification subproblem (22) with respect to x^* and y^* from Step 2, which identifies the

worst-case realization \mathbf{u}_n^* of power loads, wind generation, and gas loads that leads to the largest possible security violation.

Step 4: If the largest possible security violation identified in Step 3 is no larger than v^{\max} , x^* and y^* are final solutions and the process terminates; Otherwise, set n=n+1, introduce new variables z_n and v_n and new constraints (24) to the master problem (20), and go back to Step 2.

$$f^{\mathrm{T}} \mathbf{v}_n \le \mathbf{v}^{\mathrm{max}} \tag{24a}$$

$$Cx + Dy + Ez_n + Gv_n \le h - Hu_n^*$$
(24b)

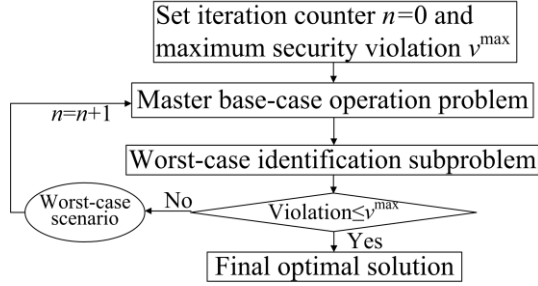


Fig. 2. Flowchart of the CCG algorithm.

4. Numerical Results

In this section, a 6-bus power system with a 7-node natural gas system and a modified IEEE 118-bus power system with a 12-node natural gas system are used to demonstrate effectiveness of the proposed two-stage adjustable robust co-optimization model. Test data are modified based on [13] and [16]. Wind spillage cost, power load shedding cost, and gas load shedding cost are set as \$100/MWh, \$1000/MWh, and \$4104/kcf (or equivalently \$4000/MWh), respectively. Specifically, natural gas load shedding cost is much higher than that of power load, in order to reflect the fact that residential gas loads have a higher priority than gas-fired units. All case studies are solved by Gurobi 6.5 on a personal computer with Intel Core i7 3.6 GHz processor and 16 GB memory. Number of breakpoints *K* in Section 4.1 is set as 100 for all pipelines as a trade-off between computational time and solution accuracy.

4.1 6-Bus Power System/7-Node Natural Gas System

In this section, a 6-bus power system with a 7-node natural gas system shown in Fig. 3 is used to demonstrate effectiveness of the proposed approach. The 6-bus power system includes three non-gas units G2-G4, one gas-fired unit G1 connected to gas node 3, one dual-fuel unit G5 connected to gas node 1, one

wind farm, seven transmission lines, and three electrical loads (besides gas compressor). Peak power demand is 480 MW. Capacity and forecasted peak wind generation of the wind farm are 120MW and 97.8MW, respectively. Fuel price of non-gas-fired units is 4\$/MBtu.

The 7-node natural gas system includes two gas wells, one gas storage, one active pipeline, five passive pipelines, and three gas loads. Peak gas demand is 7342 kcf/h. The active pipeline 2-4 is equipped with an electric-driven compressor, which is connected to bus 4 of the power grid with fuel consumption factor of 0.03 [27]. The PtG facility, connected at bus 4 of the power grid and at node 2 of the gas network, has a capacity of 37.5MW and efficiency of 0.64 [2], [16]. Initial and terminal linepack of the entire gas system are both set as 106800kcf to facilitate daily operation. Production costs of the two gas wells are 3\$/kcf and 3.6\$/kcf, respectively. Operation cost of the gas storage is 0.5\$/kcf.

Profiles of forecasted electricity loads, wind generation, and gas loads are shown in Fig. 4. Variations of electric power loads, wind generation, and gas loads are considered as 10%,

20%, and 10% of their forecast values, i.e.,
$$\tilde{I}$$
 $\frac{b}{dt}$,

$$\tilde{I}$$
 P_{wt}^b , and \tilde{I} P_{gt}^b in (14b)-(14d). Budgets of uncertainties Δ_d , Δ_w , and Δ_g are all set as 24. System operation security violation threshold v^{\max} is set to \$0.01,

which ensures negligible power/gas load shedding and wind spillage under uncertainties. Threshold of relative MILP gap is set as 0.01%.

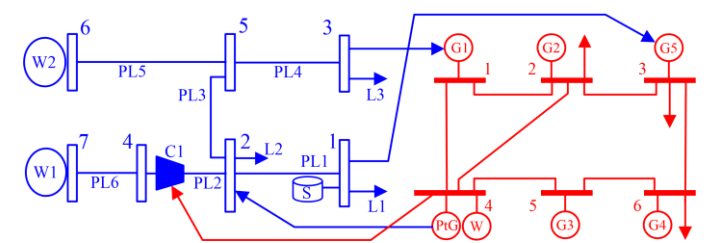


Fig. 3. 6-bus power system/7-node natural gas system.

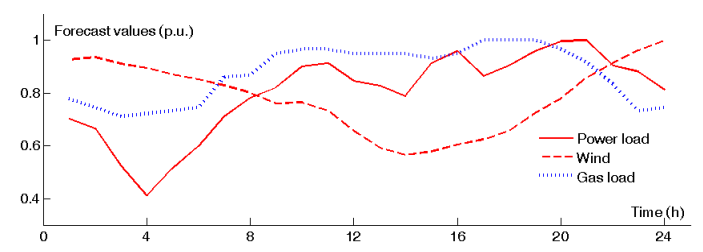


Fig. 4. Profiles of forecasted power loads, wind generation, and gas loads.

The following six cases are studied to illustrate the proposed robust day-ahead scheduling approach of IPGS. The main settings of different cases are compared in Table I.

Case 1: Co-optimization without uncertainties. This is the base case for comparison with other cases.

Case 2: Robust co-optimization with uncertainties. The influence of system uncertainties on the IPGS is tested in this case.

Cases 3-4: Cases 1-2 with natural gas system congestion, in which gas loads L1 and L3 are both increased by 10% of total original residential gas loads. These

two cases are studied to show the impact of gas network congestion on the operation of electric power system.

Case 5: Case 4 with fuel-switching limit of dual-fuel units. The effect of fuel-switching limits on the optimal scheduling of IPGS is simulated in this case.

Case 6: Case 4 with different wind penetration levels. In this case, the impact of different wind penetration levels on the optimal scheduling of IPGS is studied.

Table I Comparison of different settings in Cases 1-6

Case U	ncertainties	Gas system congestions	Fuel-switching limits	Different wind penetration levels
1	N	N	N	N
2	Y	N	N	N
3	N	Y	N	N
4	Y	Y	N	N
5	Y	Y	Y	N
6	Y	Y	N	Y

Cases 1-4: Fig. 5 shows results of unit commitment of G4 and G5 and flow direction of pipeline PL3 in Cases 1-4. In these four cases, the cheapest units G1 and G2 are always committed in all 24 hours, the most expensive unit G3 stays off for the entire day, and gas flows of all pipelines except PL3 keep the same direction throughout the day. Thus, they are not reported in Fig. 5. Solid circles in Fig. 5 represent that units are ON and gas flows are in positive direction. In addition, black stars in Case 4 describe that dual-fuel units burn traditional fuel instead of natural gas. Total operation costs of the IPGS, total gas consumption of G1 and G5, and power consumption of the gas compressor in the four cases are shown in Table II.

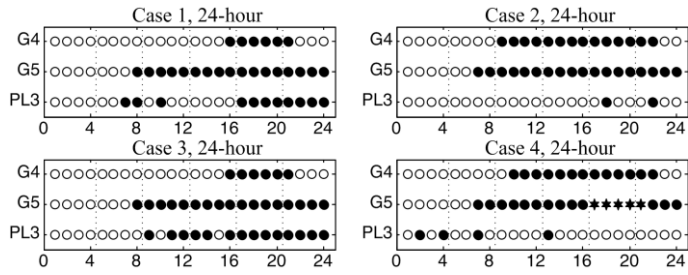


Fig. 5. UC solutions and gas flow directions for Cases 1-4.

In Case 1 where uncertainties and natural gas system congestions are neglected, G4 is committed in hours 16-21, G5 is committed in hours 8-24, and pipeline PL3 has positive gas flow direction in hours 7-8, 10, and 17-24. When uncertainties are considered in Case 2, total cost increases to \$M0.913 because more generating units are committed and pipeline PL3 has negative gas flows in 22 hours. In this case, transmission line limits are binding under the worst-case scenarios which could cause electric load shedding. Specifically, compared with Case 1, G4 is turned on in extra hours of 9-15 and 22 while G5 is also turn on at hour 7, which contribute to mitigating power load shedding induced by electricity transmission violations and/or shortage of ramping capabilities in the worst-case scenarios at hours 7-15 and 23. As non-gas-fired units are turned on more extensively, total gas consumption of G1 and G5 throughout the day is decreased from 77226.48kcf to

76834.72kcf as shown in Table II. Consequently, gas production of gas wells is reduced by 410.58kcf, and electric energy consumed by the gas compressor is reduced by 19.85MWh. As for the natural gas network, gas well W1 alone cannot fully support gas loads L1, L2, and G5 in worst-case scenarios. That is, the gas network relies on gas well W2 to produce gas for meeting part of gas loads L1, L2, and G5. As a result, gas flow of pipeline PL3 is directed from node 5 to node 2 in 22 out of 24 hours.

Table II Comparison of results in Cases 1-4

Case	Total cost	Total gas consumption	Electric energy consumption of
	(\$)	of G1 and G5 (kcf)	the gas compressor (MWh)
1	909105.10	77245.30	1025.16
2	912861.99	76834.72	1005.31
3	1022288.63	69085.32	1025.82
4	1027229.07	67839.65	1015.69

When natural gas network congestion appears in Case 3 with increased residential gas loads, pressures of some gas nodes have reached their lower or upper bounds. In this case, unit commitment solution of generators remains the same as that in Case 1, while gas flow direction of pipeline PL3 differs slightly. Table II shows that, because natural gas network congestion does not occur in Case 1 and natural gas is cheaper than traditional fuel, gas-fired units and dual-fuel units burn as much gas fuel as possible to generate electricity. In comparison, in Case 3, gas consumption of G1 and G5 is reduced because higher-priority residential gas loads L1 and L3 have to be served first.

However, when uncertainties are further considered in Case 4, natural gas network congestion presents more significant impacts on power system operation as shown in Fig. 5. Specifically, in Case 4, pipeline PL1 is congested in worst-case scenarios due to nodal pressure limits, which causes insufficient gas supply to dual-fuel unit G5. In turn, dual-fuel unit G5 is switched to burn traditional fuel for meeting electricity demands in hours 17-21, when power and gas demands reach their peaks concurrently. Results of Case 4 show that dual-fuel units can effectively shave natural gas consumption at peak hours by switching to other fuels.

As stochastic programming is also recognized as an effective approach for handling uncertainties in optimization problems [38]-[39], solutions of the proposed robust model and the stochastic programming model are further compared. Specifically, in the stochastic programming model, uncertainties of electrical loads, wind power generations, and gas loads are assumed to follow uniform distributions within predefined uncertainty sets. 5000 scenarios are generated via the Latin hypercube sampling method for simulating these uncertainties in a 24-hour period, which is further reduced to 5 scenarios via scenario reduction techniques as a trade-off between computational speed and solution quality [38]. Results of stochastic programming models corresponding to Cases 2 and 4 are compared in Table III. It is observed that results obtained by stochastic programming yield a smaller base-case cost for covering high-probability scenarios, while the system may be vulnerable to low-probability high-impact worst cases with relatively higher system load shedding. Specifically, in Case 4 where natural gas network is congested, inefficient scheduling solution from stochastic programming increases the

worst-case operation cost by 65% as compared to the solution from robust optimization. Indeed, the proposed robust day-ahead scheduling of IPGS greatly enhances operational security of interdependent systems with a reasonable increase in base-case operation cost.

Table III Comparison of results from robust optimization and stochastic programming

Case	Base-case total cost (\$)	Worst-case total cost (\$)	Worst-case load shedding cost (\$)
2 (robust)	912861.99	1030610.56	0
2 (stochastic)	909988.93	1041209.93	11718.98
4 (robust)	1027229.07	1192797.45	0
4 (stochastic)	1023258.22	1966687.99	829214.37

Cases 5: In this case, limit on the number of fuel switches of dual-fuel unit G5 is set as 0, 1, 2, and 3 (denoted as Cases 5.1-5.4), to explore influence of fuel-switching limits. Unit commitment solutions of G4 and G5 in these cases are shown in Fig. 6, while total costs and gas consumptions of G5 are presented in Table IV. Unit commitment statuses of G1-G3 are the same as those in Cases 1-4.

6 shows that fuel-switching limit influences commitment statuses of peaking units G4 and G5. Specifically, because switching fuel is forbidden in Case 5.1, G5 is only committed in hours 10-24 because of limited gas fuel supply. which triggers G4 to be committed between hours 7-23 for ensuring operational security of power systems. In Case 5.2, G5 switches to burn traditional fuel in hours 18-24 when natural gas demand is relatively high, and G4 is only needed in hours 10-22. Moreover, when fuel-switching limit is larger than 1, unit commitment solutions in Cases 5.3 and 5.4 do not change anymore. In addition, as shown in Table IV, in the worst-case scenario, natural gas supply to G5 is more restricted because most available natural gas is used to supply high residential gas demands. Table IV also indicates that a larger fuel-switching limit will result in a more economical system operation scheduling. In summary, fuel-switching capabilities of dual-fuel units play an important role in supporting the secure and economical operation of IPGS with gas supply shortage.

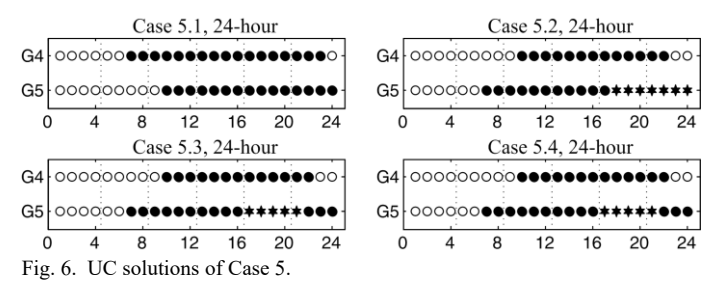


Table IV Total cost and gas consumption of G5 in Case 5

Case	Total cost (\$)	Base-case gas consumption of G5 (kcf)	Worst-case gas
	(-)	1 ' '	consumption of G5 (kcf)
5.1	1029910.86	11628.36	8106.58
5.2	1027514.33	8008.79	6880.91
5.3	1027229.07	10860.39	9396.19
5.4	1027229.07	10860.39	9396.19

Cases 6: Impact of different wind penetration levels, including 18%, 20%, and 22% (denoted as Case 6.1-6.3), is further

examined. Moreover, influence of PtG is also explored via Case 6.4 by increasing the capacity of PtG from 37.5MW in Case 6.3 to 50MW. Unit commitment solutions of all five units are presented in Fig. 7.

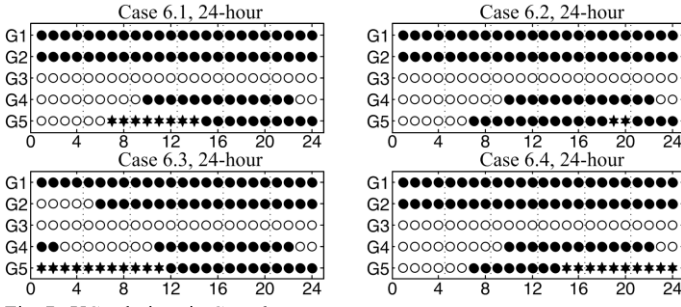


Fig. 7. UC solutions in Case 6.

As shown in Fig. 7, increasing wind penetration level from 18% to 20% only impacts operation status of G5, in terms of a larger numbers of hours to burn traditional fuel. Moreover, when wind penetration increases to 22%, minimum output constraints of G1 and G2 will trigger wind spillage in the worst-case scenario. As a result, G2 is turned off in hours 1-5 so that wind spillage could be avoided under uncertainties. In comparison, when capacity of PtG is increased to 50MW in Case 6.4, base unit G2 can be kept online in the early morning for providing a more economical scheduling solution. That is, PtG can effectively provide ramping down capabilities for power systems to prevent wind spillage, by converting excessive wind energy into natural gas. In turn, with a better operation scheduling, a more effective utilization of uncertain wind generation can be guaranteed, while total operation cost is also reduced from \$M0.980 in Case 6.3 to \$M0.974 in Case 6.4.

4.2 IEEE 118-Bus Power System/12-Node Gas System

A modified IEEE 118-bus power system together with a 12-node natural gas system is applied here to further demonstrate applicability of the proposed model on larger systems. The modified IEEE-118 bus power system includes 46 non-gas thermal units, 6 gas-fired units, 2 dual-fuel units, 7 wind farms, 1 PtG facility, 186 branches, and 91 power loads. Total capacities of gas-fired units, dual fuel units, and wind farms are 525MW, 200MW, and 720MW, respectively.

The gas system consists of 12 gas nodes, 3 gas wells, 10 inactive pipelines, 2 active pipelines with gas compressors, 2 storage facilities, and 12 gas loads. The PtG facility is connected to power bus 4 and gas node 4. Two electric-driven gas compressors draw electric power from buses 7 and 15 of the power grid. Forecasted values of peak power load, wind generation, and gas load are 6000MW, 635MW, and 9000kcf/h, respectively.

With threshold on relative MILP gap of 0.1%, the deterministic co-optimization model without uncertainties is solved in 60s. In this IPGS, cheaper gas-fired units G1 and G2 are not constantly operated at their full capacities due to natural gas shortage. Furthermore, lower linepack in some pipelines at the beginning of the day has limited natural gas supply to gas-fired units G1/G2 and dual-fuel units G4/G5, because residential gas demands at nodes 4, 6, and 7 are given higher priority to be served. As a result, G1 and G2 are forced to shut

down in the early morning until linepack in pipelines is refilled later of the day. However, fuel-switching capabilities of G4 and G5 allow them to continue operation while relying on traditional fuel. In this case without considering uncertainties, total operation cost is \$M6.230 with a total of 651 unit hour commitment throughout the day.

When considering uncertainties in the adjustable robust model, calculation time increases significantly to 3627s due to computational burden of the robust optimization [17], [21]. Furthermore, in order to maintain power system security, 59 more unit hour are committed throughout the day to provide enough up/down ramping capabilities for handling worst-case scenarios, which yields a total operation cost of \$M6.234. In addition, to ensure operational security of the natural gas system in the worst-case scenario, total natural gas consumption of gas-fired and dual-fuel units G1-G8 is decreased from M0.242kcf in the deterministic case to M0.194kcf.

5. Conclusions

This paper proposes a two-stage adjustable robust model for the coordinated optimal operation of the IPGS, while considering uncertainties of power loads, wind generation, and gas loads. Coupling components including gas-fired units, dual-fuel units, PtGs, and electric-driven compressors are studied. The proposed two-stage robust optimization model is solved by CCG, in which nonlinear gas network constraints are linearized via Taylor series expansion.

Simulation results show that system uncertainties need to be adequately considered in order to derive accurate unit commitment solutions and gas flow directions of the IPGS. In addition, fuel-switching capabilities of dual-fuel units are valuable in enhancing the secure and economical operation of IPGS, especially when natural gas demands present upward uncertainties. Moreover, PtG facilities can positively contribute to a more economical unit commitment scheduling by effectively converting excessive wind generation into natural gas, while also facilitating a deeper penetration of wind energy. In summary, the proposed approach provides a physically secure and economically viable solution to optimally operate IPGS against various upcoming uncertainties.

Acknowledgments

This work was supported in part by the U.S. National Science Foundation grants ECCS-1254310 and CMMI-1635339, and in part by the Science and Technology Bureau of Sichuan Province, China grant 2017HH0053 in collaboration with University of Electronic Science and Technology of China.

References

- EIA, Monthly Energy Review, 2016, [Online]. Available: http://www.eia.gov/totalenergy/data/monthly/#naturalgas/.
- [2] Jentsch M, Trost T, Sterner M. Optimal use of power-to-gas energy storage systems in an 85% renewable energy scenario. Energy Procedia 2014; 46: 254-261.
- [3] Clegg S and Mancarella P. Integrated modeling and assessment of the operational impact of power-to-gas (P2G) on electrical and gas transmission networks. IEEE Trans Sustain Energy 2015; 6(4):1234-1244.

- [4] Shahidehpour M, Fu Y, and Wiedman T. Impact of natural gas infrastructure on electric power systems. Proc IEEE 2005; 93(5): 1042-1056.
- [5] Li T, Eremia M, and Shahidehpour M. Interdependency of natural gas network and power system security. IEEE Trans Power Syst 2008: 23(4): 1817-1824.
- [6] Liu C, Shahidehpour M, Fu Y, and Li Z. Security-constrained unit commitment with natural gas transmission constraints. IEEE Trans Power Syst 2009; 24(3): 1523-1536.
- [7] Martínez-Mares A and Fuerte-Esquivel C. A unified gas and power flow analysis in natural gas and electricity coupled networks. IEEE Trans Power Syst 2012; 27(4): 2156-2166.
- [8] Correa-Posada C and Sanchez-Martin P. Integrated power and natural gas model for energy adequacy in short-term operation. IEEE Trans Power Syst 2015; 30(6): 3347-3355.
- [9] Zeng Q, Fang J, Li J, and Chen Z. Steady-state analysis of the integrated natural gas and electric power system with bi-directional energy conversion. Appl Energy 2016; 184:1483-1492.
- [10] Li G, Zhang R, Jiang T, Chen H, Bai L, and Li X. Security-constrained bi-level economic dispatch model for integrated natural gas and electricity systems considering wind power and power-to-gas process. Appl Energy 2017; 194: 696-704.
- [11] Wu L and Shahidehpour M. Optimal coordination of stochastic hydro and natural gas supplies in midterm operation of power systems. IET Gener Transm Distrib 2011; 5(5): 577-587.
- [12] Alabdulwahab A, Abusorrah A, Zhang X, and Shahidehpour M. Coordination of interdependent natural gas and electricity infrastructures for firming the variability of wind energy in stochastic day-ahead scheduling. IEEE Trans Sustain Energy 2015; 6(2): 606-615.
- [13] Zhang X, Shahidehpour M, Alabdulwahab A, and Abusorrah A. Hourly electricity demand response in the stochastic day-ahead scheduling of coordinated electricity and natural gas networks. IEEE Trans Power Syst 2016; 31(1): 592-601.
- [14] Shams M, Shahabi M, and Khodayar M. Stochastic day-ahead scheduling of multiple energy Carrier microgrids with demand response. Energy 2018; 155:326-338.
- [15] Qiao Z, Guo Q, Sun H, et al. An interval gas flow analysis in natural gas and electricity coupled networks considering the uncertainty of wind power. Appl Energy 2017; 201:343-353.
- [16] He C, Wu L, Liu T, and Shahidehpour M. Robust co-optimization scheduling of electricity and natural gas systems via ADMM. IEEE Trans Sustain Energy 2017; 8(2):658-670.
- [17] He C, Liu T, Wu L, and Shahidehpour M. Robust coordination of interdependent electricity and natural gas systems in day-ahead scheduling for facilitating volatile renewable generations via power-to-gas technology. J Modern Power Syst Clean Energy 2017; 5(3):375-388.
- [18] Lu B and Shahidehpour M. Unit commitment with flexible generating units. IEEE Trans Power Syst 2005; 20(2): 1022-1034.
- [19] Zeng B and Zhao L. Solving two-stage robust optimization problems using a column-and-constraint generation method. Operations Research Lett 2013; 41(5): 457-461.
- [20] Hu B, Wu L, and Marwali M. On the robust solution to SCUC with load and wind uncertainty correlations. IEEE Trans Power Syst 2014; 29(6): 2952-2964.
- [21] Dai C, Wu L, and Wu H. A multi-band uncertainty set based robust SCUC with spatial and temporal budget constraints. IEEE Trans Power Syst 2016; 31(6): 4988-5000.
- [22] Ben-Tal A, Goryashko A, Guslitzer E, and Nemirovski A. Adjustable robust solutions of uncertain linear programs. Math Program 2004; 99(2): 351-376.
- [23] NERC, Short-term special assessment operational risk assessment with high penetration of natural gas-fired generation, 2016, [Online]. Available:http://www.nerc.com/pa/RAPA/ra/Reliability%20Assessment s%20DL/NERC%20Short-Term%20Special%20Assessment%20Gas%2 0Electric Final.pdf.
- [24] Department of Energy, Strategic energy analysis and planning, 2015, [Online]. Available: https://energy.gov/sites/prod/files/2015/09/f26/ SEAP TLF.pdf.
- [25] US DOT PHMSA, Guidance for pipeline flow reversals, product changes, and conversion to service, 2014, [Online]. Available: http://www.oc ceweb.com/PLS/2014Gas/Guide-Flo%20Rev-Prod%20Ch-Conver.pdf.
- [26] Wang C, Wei W, Wang J, Bai L, and Liang Y. Distributed optimal gas-power flow using convex optimization and admm. (2016). [Online]. Available: https://arxiv.org/abs/1610.04681

- [27] Wu S, Rios-Mercade R, Boyd E, and Scott L. Model relaxation for the fuel cost minimization of steady-state gas pipeline networks. Math Comput Model 2000; 31(2-3): 197-220.
- [28] Menon E, Gas Pipeline Hydraulics. Boca Raton, FL, USA: Taylor & Francis, 2005.
- [29] Amirnekooei K, Ardehali M, and Sadri A. Optimal energy pricing for integrated natural gas and electric power network with considerations for techno-economic constraints. Energy 2017; 123: 693-709.
- [30] Clegg S, and Mancarella P. Integrated electricity-heat-gas modelling and assessment, with applications to the Great Britain system. Part II: Transmission network analysis and low carbon technology and resilience case studies. Energy 2018 (to appear).
- [31] Ahmadian H, Boozarjomehry R. Dynamic optimization of natural gas networks under customer demand uncertainties. Energy 2017;134:968-983.
- [32] Tomasgard A, Rømo F, Fodstad M, and Midthun K. Optimization models for the natural gas value chain. Geom Model Numer Simul Optimiz 2007; 521-558.
- [33] Bailera M, Lisbona P. Energy storage in Spain: Forecasting electricity

- excess and assessment of power-to-gas potential up to 2050. Energy 2018:143:900-910.
- [34] Qadrdan M, Abeysekera M, Chaudry M, Wu J, and Jenkins N. Role of power-to-gas in an integrated gas and electricity system in Great Britain. Int J Hydrog Energy 2015; 40(17): 5763-5775.
- [35] Jiang R, Wang J, and Guan Y. Robust unit commitment with wind power and pumped storage hydro. IEEE Trans Power Syst 2012; 27(2): 800-810.
- [36] Zhao C, Wang J, Watson J, and Guan Y. Multi-stage robust unit commitment considering wind and demand response uncertainties. IEEE Trans Power Syst 2013; 28(3): 2708-2717.
- [37] Midthun K, Bjørndal M, Tomasgard A. Modeling Optimal Economic Dispatch and System Effects in Natural Gas Networks. Energy J 2009;30:155–80.
- [38] Alvarez Lopez J, Ponnambalam K, and Quintana V. Generation and transmission expansion under risk using stochastic programming. IEEE Trans Power Syst 2007; 22: 1369-1378.
- [39] Wang J, Shahidehpour M, and Li Z. Security-constrained unit commitment with volatile wind power generation. IEEE Trans Power Syst 2008; 23: 1319-1327.